NASA/TP—1999–209264

Contamination Effects on EUV Optics

J. Tveekrem
Goddard Space Flight Center, Greenbelt, MD

National Aeronautics and
Space Administration

Marshall Space Flight Center • MSFC, Alabama 35812

June 1999

Available from:

NASA Center for AeroSpace Information
800 Elkridge Landing Road
Linthicum Heights, MD 21090–2934
(301) 621–0390

National Technical Information Service
5285 Port Royal Road
Springfield, VA 22161
(703) 487–4650

TABLE OF CONTENTS

INTRODUCTION 1

OPTICAL EFFECTS OF PARTICULATE CONTAMINATION 1

- Scatterometer Design 2
- Experiment Description 4
- OPALS Model 6
- Results 6
- Conclusion 15

OPTICAL EFFECTS OF MOLECULAR CONTAMINATION 15

- Contamination Irradiation Facility 17
- Results 19
- Conclusion 26

REFERENCES 31

LIST OF FIGURES

1. Schematic diagram of scatterometer 3

2. Measured and theoretical BRDF distributions at 6328 Å and normal incidence. Distributions 1 and 2 are shown in Table 1(a) and (b) respectively 7

3. Measured and theoretical BRDF distributions at 325 nm and normal incidence. Distributions 1 and 2 are shown in Table 1(a) and (b) respectively 9

4. Measured and theoretical data, for 121.6 nm and −15 degree angle of incidence. The measured data shows both positive and negative $\beta - \beta_0$ 11

5. Measured and theoretical data for 74.0 nm and −15 degree angle of incidence. The measured data shows both positive and negative $\beta - \beta_0$ 13

6. Measured BRDF data for the same sample at four different wavelengths. Data are shown for positive and negative $\beta - \beta_0$ 14

7. UV reflectance at normal incidence 16

8. Schematic diagram of contamination irradiation facility 18

9. In-situ reflectance measurements of an Al + MgF_2 mirror before contamination and after contamination + irradiation. Measurements were also made after contamination but before irradiation, and no change in reflectance was seen compared to the uncontaminated state 20

10. Reflectance change of Al + MgF_2 mirror. No contamination introduced 22

11. Reflectance change of Al + MgF_2 mirror. No contamination introduced 23

12. Reflectance change of Al + MgF_2 mirror. Contaminant: Epon 815C/Versamid 140 24

13. Reflectance change of Al + MgF_2 mirror. Contaminant: Braycote 601 25

14. Reflectance change of Al + MgF_2 mirror. Contaminant: Rheolube 2000 27

15. Reflectance change of Al + MgF_2 mirror. Contaminant: Pennzane X–2000 28

16. Reflectance change of Al + MgF_2 mirror. Contamination: Krytox 240 AC 29

LIST OF TABLES

1. (a) and (b) represent particulate distributions measured at two different points on the sample under investigation 5

2. Optical constants of carbon and silicon dioxide at measured visible wavelengths 8

3. Optical constants of carbon and silicon dioxide at measured EUV wavelengths 12

INTRODUCTION

During ground-based assembly and upon exposure to the space environment, optical surfaces accumulate both particulates and molecular condensibles, inevitably resulting in degradation of optical instrument performance.

Currently, this performance degradation (and the resulting end-of-life instrument performance) cannot be predicted with sufficient accuracy using existing software tools. Optical design codes exist to calculate instrument performance, but these codes generally assume uncontaminated optical surfaces. Contamination models exist which predict approximate end-of-life contamination levels, but the optical effects of these contamination levels can not be quantified without detailed information about the optical constants and scattering properties of the contaminant. The problem is particularly pronounced in the extreme ultraviolet (EUV, 300-1200 Å) and far ultraviolet (FUV, 1200-2000 Å) regimes due to a lack of data and a lack of knowledge of the detailed physical and chemical processes involved. Yet it is in precisely these wavelength regimes that accurate predictions are most important, because EUV/FUV instruments are extremely sensitive to contamination.

OPTICAL EFFECTS OF PARTICULATE CONTAMINATION

Considerable experimental and theoretical work has already been done on contamination effects in the visible and IR spectral regions. These include measurements by Spyak and Wolfe[1] and Carosso and Carosso[2], among others. The first attempt at modelling these effects was made by Young[3], who adopted a Mie theory approach to successfully predict the scatter from a distribution of silver spheres on a mirror for λ = 0.6328 μm and 10.6 μm. Most subsequent models have built upon this ground-breaking work by Young. One more recent approach, which has met with some success in the IR region, is that adopted by Whitlock and Jackson[4]. This basically considers the problem of scatter from a spherical particle on a substrate as the combination of Mie scattering and classical terms such as reflection, diffraction and obscuration. The modelling effort remains active; indeed, entire sessions of optical meetings have been devoted to this subject. As pointed out by Spyak and Wolfe, however, much more effort needs to be devoted toward experimentally verifying these models. Our results provide partial verification of these models, and address the feasibility of extending these contaminant scattering theories to shorter wavelengths.

We have investigated the effects of particulate contamination on optical performance in the EUV and FUV. Specifically, we have measured the specular reflectance and Bidirectional Reflectance Distribution Function (BRDF) of deliberately-contaminated optical surfaces at several wavelengths between 740 and 6328 Å. The BRDF is defined by

$$\mathrm{BRDF} = (dP/d\Omega)/\,P_i \cos\theta_s$$

where $dP/d\Omega$ = the measured scattered power per unit solid angle,
P_i = the incident power on the sample, and
θ_s = the scattering angle.

BRDF measurements have not previously been performed in this region of the spectrum because of the necessity for making the measurements in vacuum. Thus our data are entirely new. Our investigation involved both experimental measurements under vacuum conditions and theoretical modelling of the reflectance and scattering process.

Scatterometer Design

The experimental apparatus used was an EUV scatterometer which we designed. Details of the scatterometer design have been published elsewhere.[5] A description is given here. The instrument has three basic elements: a light source, a sample mount, and a detector. Because of the EUV wavelengths being measured, all of these elements must be maintained under vacuum.

The specific geometry of the scatterometer is shown schematically in Figure 1. It is based around a reflectometer similar to that of Hunter[6], modified to accommodate plane-of-incidence scatter measurements.

The EUV light source used for these investigations was a duoplasmatron. The advantage that the duoplasmatron source enjoys when compared with a conventional hot-filament light source is that the discharge is constricted and concentrated by application of a magnetic field, resulting in a narrower, more intense beam along the axis of the source-to-collector.

The output of the source is directed into a McPherson model 247, Rowland-circle-mount, grazing-incidence monochromator. After emerging from the exit slit of the monochromator, the beam is then quasi collimated by being passed through two small circular apertures (typically 1 mm in diameter.) After passing through the apertures, the beam enters the sample chamber. The spot size at the sample is determined by the diameter of the collimation apertures. In general the spot on the sample is rectangular in shape and is between 1 and 2 mm in extent.

The sample can be rotated about a vertical axis to allow different angles of incidence, and the detector can be rotated independently about the same axis to allow the angular scatter distribution to be measured. Changes in angle of incidence and detector position were performed manually, and they could be set nominally to ±0.05°.

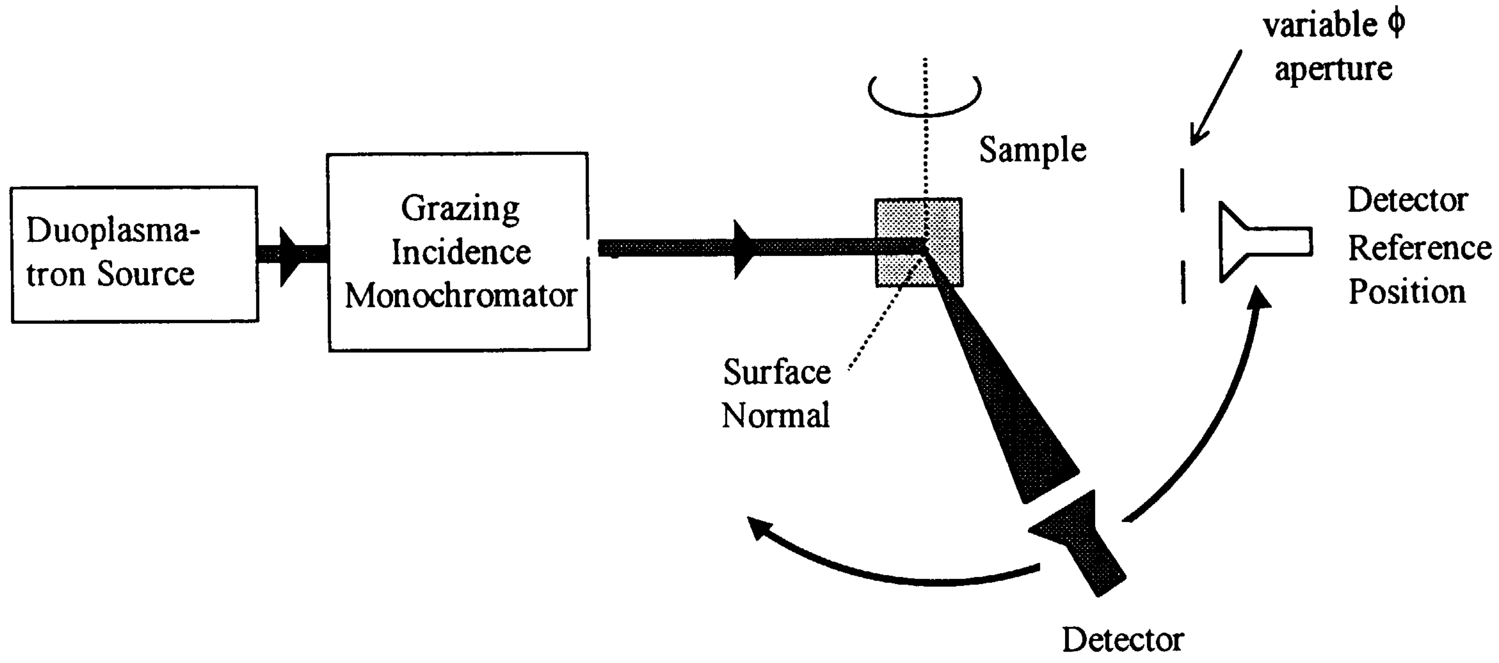

Figure 1 - Schematic Diagram of Scatterometer

One of the major problems encountered in performing BRDF measurements is that the detector must be extremely sensitive in order to measure low-intensity wide-angle scatter, yet must also be capable of measuring the full unobstructed beam power. That is, the detector must have a very large dynamic range. The detector used was a Galileo dual-mode 4930 Channeltron. This particular detector was chosen because of its almost unique qualities at these wavelengths of combining low-light-level sensitivity, i.e., good quantum efficiency, with large dynamic range (7-8 orders of magnitude.)

The detector consisted of two sections. The front section was a low-gain current measurement device, and it was used for measuring high intensities such as the full incident beam power. An electrometer was used to make the current measurements. For measuring low light levels, the output of the front section was directed into the rear high-gain photon-counting section, providing further amplification. A multichannel analyzer was used to make the photon counting measurements.

Experiment description

The sample under investigation was a MgF_2 protected aluminum coating optimized for high reflectance at 1216 Å. The micro-roughness of the surface was measured with a Wyko Topo-3D profilometer, employing a 10X head, and was found to be less than 10 Å rms. Smooth mirrors are required so that the scatter from the surface micro-roughness will be small by comparison with the particulate scatter.

The sample was then exposed unprotected to the ordinary lab environment for a period of approximately one year. The exact chemical composition of the dust particulates is unknown. While, at first glance, investigating a sample whose contaminants are not well defined may seem like a strange approach to take, it should be pointed out that at EUV wavelengths the optical constants of many materials are either unknown or poorly defined. Hence, knowledge of the contaminant does not necessarily yield a great deal of further information or insight.

Particulate distribution measurements were performed with an automated Olympus microphotography system. This instrument measures the number of particles greater than a user-set size threshold, with a lower limit of about 2μm. After capturing the surface image, image analysis software allows a distribution to be obtained which gives the number of particles contained within certain bin sizes. Two such distributions for this sample are shown in Table 1. The two distributions correspond to measurements made at different points on the sample. Distribution 1 (shown in Table 1a) was measured away from the sample center, whereas distribution 2 (shown in Table 1b) was measured at the sample center. The area sampled in each case was 20.25 mm^2. Both size distributions corresponded to a MIL-STD-1246B cleanliness level of approximately 500.

Table 1 - (a) and (b) represent particulate distributions measured at two different points on the sample under investigation.

Particulate Size (μm)	No. of Particulates
2.5 - 5	5710
5 - 10	132
10 - 15	6
15 - 20	3
20 - 25	3
25 - 50	5
50 -100	1

Table 1(a)

Particulate Size (μm)	No. of Particulates
3 - 5	7089
5 - 10	363
10 - 15	18
15 - 20	2
20 - 25	3
25 - 50	3
50 -100	3

Table 1(b)

BRDF measurements were then made at four visible, NUV, FUV, and EUV wavelengths: 6328, 3250, 1216, and 740 Å. The measurements were compared with predictions from the OPALS model.

OPALS model

OPALS is an end-to-end code intended to allow parametric studies on design parameters such as sunshade geometry, system materials, temperatures, pre-launch cleanliness levels, and pointing directions. The code simulates the sun and earth as radiation sources, and particulate generation, migration, and deposition as a function of time. All of these simulations lead to a prediction of the resulting sensor degradation seen in the focal plance. A small module in the OPALS code calculates BRDF as a function of the wavelength of incident radiation, particle size distribution, and material optical properties. The approach used involves not only Mie theory, but other factors such as obscuration, reflection, refraction, and diffraction. The BRDF of a contaminated surface is assumed to be described as the sum of these terms, i.e.,

$$BRDF = BRDF_{clean} + BRDF_{mie} + BRDF_{diffr} + BRDF_{refl}$$

The model has previously been tested at infrared wavelengths[7], but not in the visible and certainly not in the EUV. One of the aims of our investigation was to evaluate the performance of this part of the OPALS code at shorter wavelengths, by comparing visible and EUV BRDF measurements with the modelling results.

Results

The detailed results of our investigation have been presented at a SPIE conference and published in the proceedings[8]. A brief summary of the results follows. Other measurements on non-contaminated optical surfaces were also published[9], these measurements demonstrate the wide utility of the EUV scatterometer.

Figure 2 shows the measured BRDF and the theoretical prediction for the BRDF plotted against scatter angle, for a wavelength of 6328 Å and at normal incidence. OPALS arrived at the theoretical BRDF values by investigating two possible contaminants with rather different optical constants, carbon and silicon dioxide[10] , which would not be uncommon in a laboratory environment. The optical constants[11] for these contaminants are shown in Table 2. The BRDF was plotted for both of the particulate distributions contained in Table 1.

Figure 3 likewise shows the measured and theoretical BRDF distributions for a wavelength of 3250 Å and at normal incidence. The theoretical curves from OPALS were obtained for the same two contaminants.

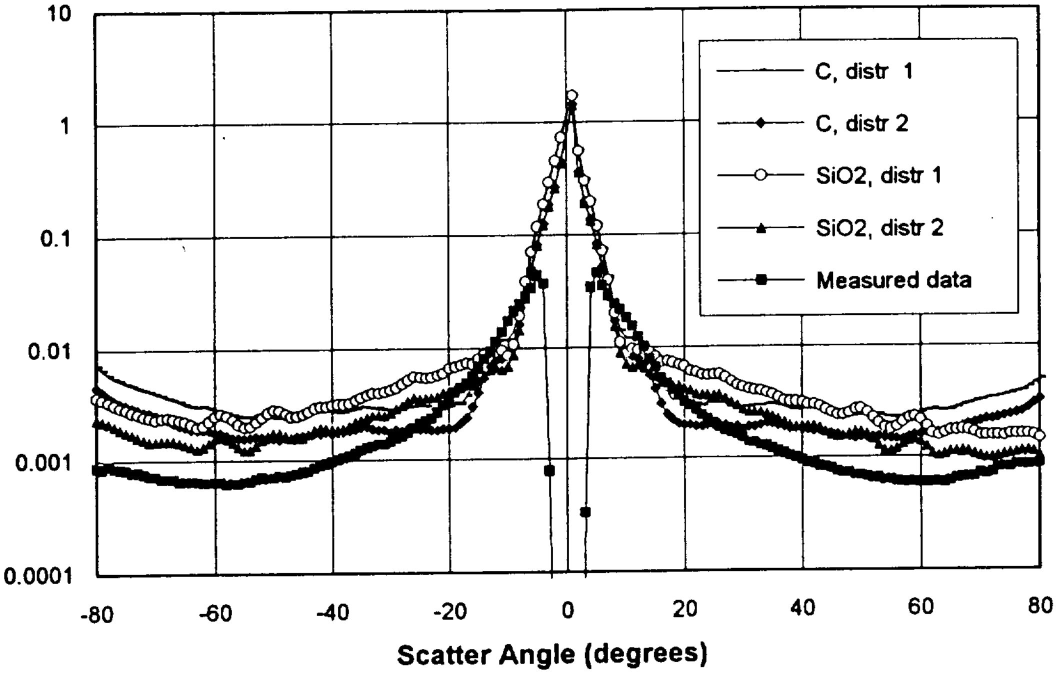

Figure 2 - Measured and theoretical BRDF distributions at 6328 Å and normal incidence. Distributions 1 and 2 are shown in Table 1(a) and (b) respectively.

Table 2 - Optical constants of carbon and silicon dioxide at measured visible wavelengths.

	Carbon		Silicon Dioxide	
Wavelength (nm)	n	k	n	k
633	2.41	1×10^{-6}	1.46	1×10^{-6}
325	2.51	7×10^{-7}	1.48	1×10^{-6}

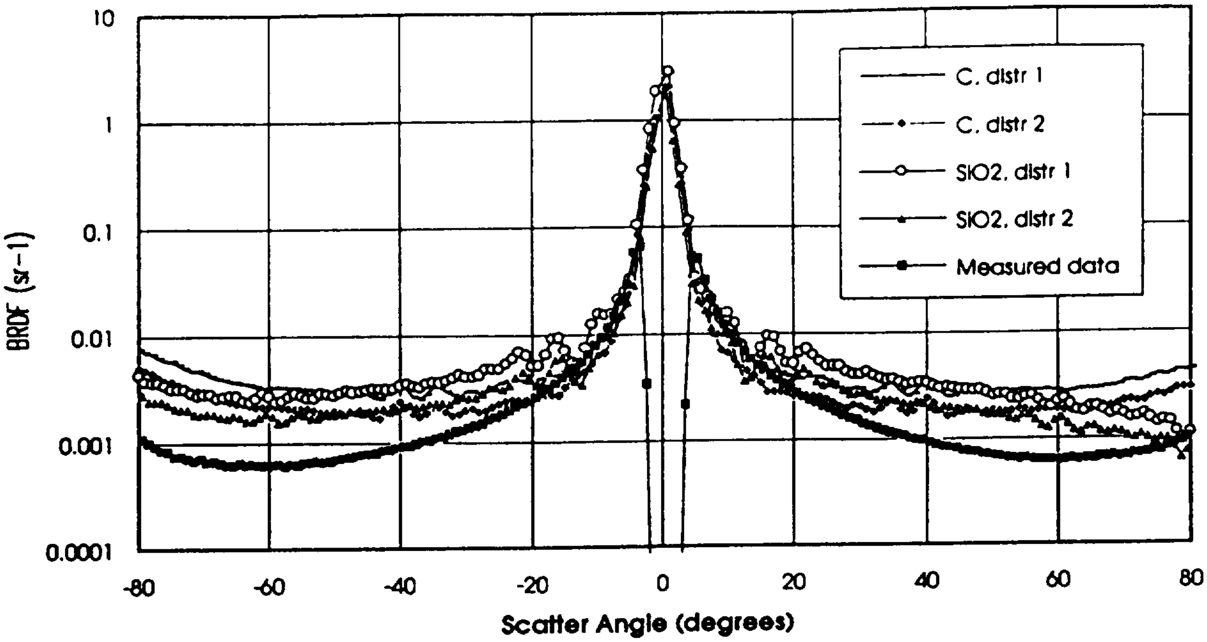

Figure 3 - Measured and theoretical BRDF distributions at 325nm and normal incidence. Distributions 1 and 2 are shown in Table 1(a) and (b) respectively.

In both Figures 2 and 3, the second particle distribution seems to fit better with the measured data than the first. Furthermore, the SiO_2 seems to model the surface better than the carbon. In summary, both figures show that the OPALS curves have the same general shape as the measured data, but the BRDF values are consistently higher than the measured data, varying between a factor of 2 and 8 depending on the particle size distribution and the optical constants used in the analysis. The theoretical curves arising from the OPALS model are always on the conservative side.

Figure 4 shows the BRDF of the contaminated sample when measured at 1216 Å, for an incident angle of -15°. Note that BRDF has been plotted against $|\beta - \beta_0| = |\sin\theta_s - \sin\theta_i|$ in order to restore near symmetry to the BRDF curves. In this case, the BRDF predictions produced by the OPALS model for the two contaminants and both distributions were practically indistinguishable. Hence, the OPALS data are shown as a single curve. The optical constants used are shown in Table 3.

Figure 5 shows the BRDF of the contaminated sample when measured at 740 Å. Again, the BRDF predictions produced by the OPALS model for both contaminants and both distributions were almost indistinguishable, and the OPALS data are shown as a single curve. The optical constants used are shown in Table 3.

Clearly, Figure 5 shows excellent agreement between the measured BRDF and the OPALS model at 740 Å, with the two curves being practically coincident beyond near specular angles. One would not expect exact agreement at near specular angles due to finite aperturing effects in the measured data. The use of a relatively large detector aperture (0.25 inches) leads to convolution of the "true" BRDF with this finite aperture, which generally leads to a broadening and lowering of the curve at near specular angles. This effect is well described by Stover[8]. Unfortunately, the large aperture was necessary in order to make the low light level far angle scatter measurements.

Figure 6 shows the BRDF of the contaminated sample at all four wavelengths: 6328, 3250, 1216, and 740 Å. In addition to agreeing with the OPALS model, the 6328, 3250, and 740 Å data also fall on top of each other, suggesting that the BRDF is wavelength-invariant. If true, this would have profound ramifications. It would mean that visible measurements of BRDF would suffice to predict EUV scatter. This would have tremendous advantages because the in situ testing of EUV scatter for most instruments is not practical due to the vacuum requirement. Furthermore, visible BRDF scatterometers employ better detector technology and more intense sources, resulting in more accurate, reliable, and repeatable measurements.

The 1216 Å data, however, are not consistent with wavelength invariance. There are some things that cause the validity of the 1216 Å data to be uncertain, but not enough to rule out the 1216 data entirely.

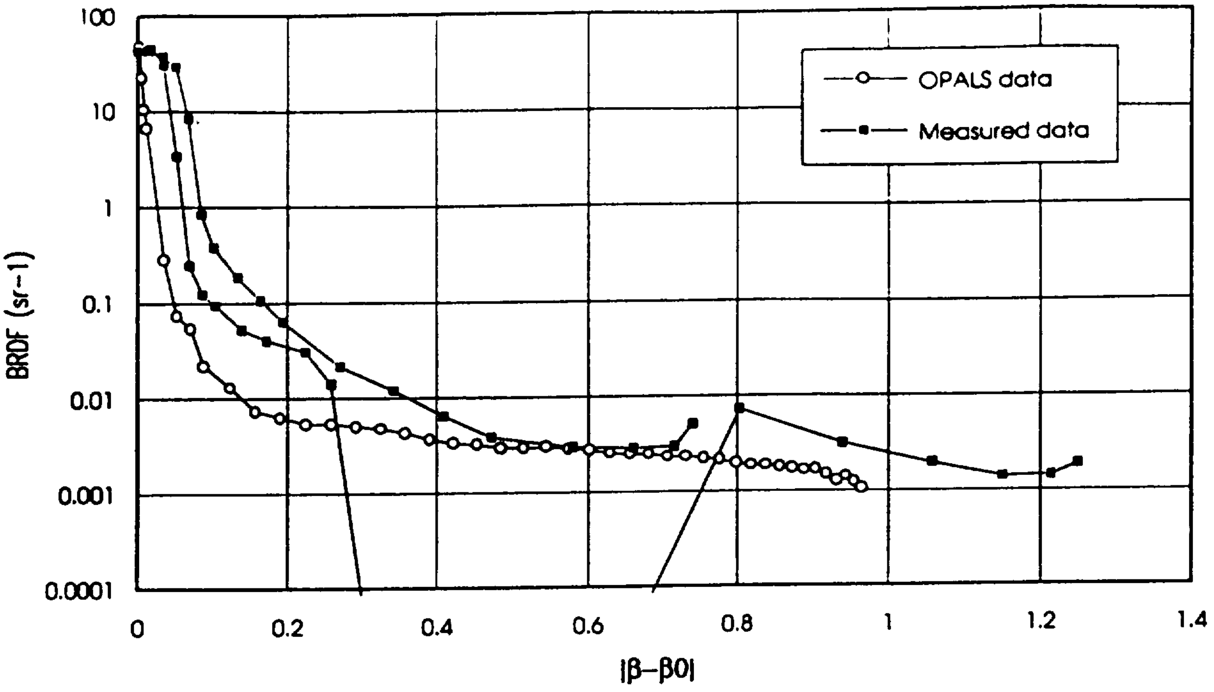

Figure 4 - Measured and theoretical data, for 121.6nm and -15 degree angle of incidence. The measured data shows both positive and negative $\beta-\beta_0$.

Table 3 - Optical constants of carbon and silicon dioxide at measured EUV wavelengths.

	Carbon		Silicon Dioxide	
Wavelength (nm)	n	k	n	k
121.6	1.80	0.44	2.24	0.715
74.0	0.836	0.793	1.124	0.765

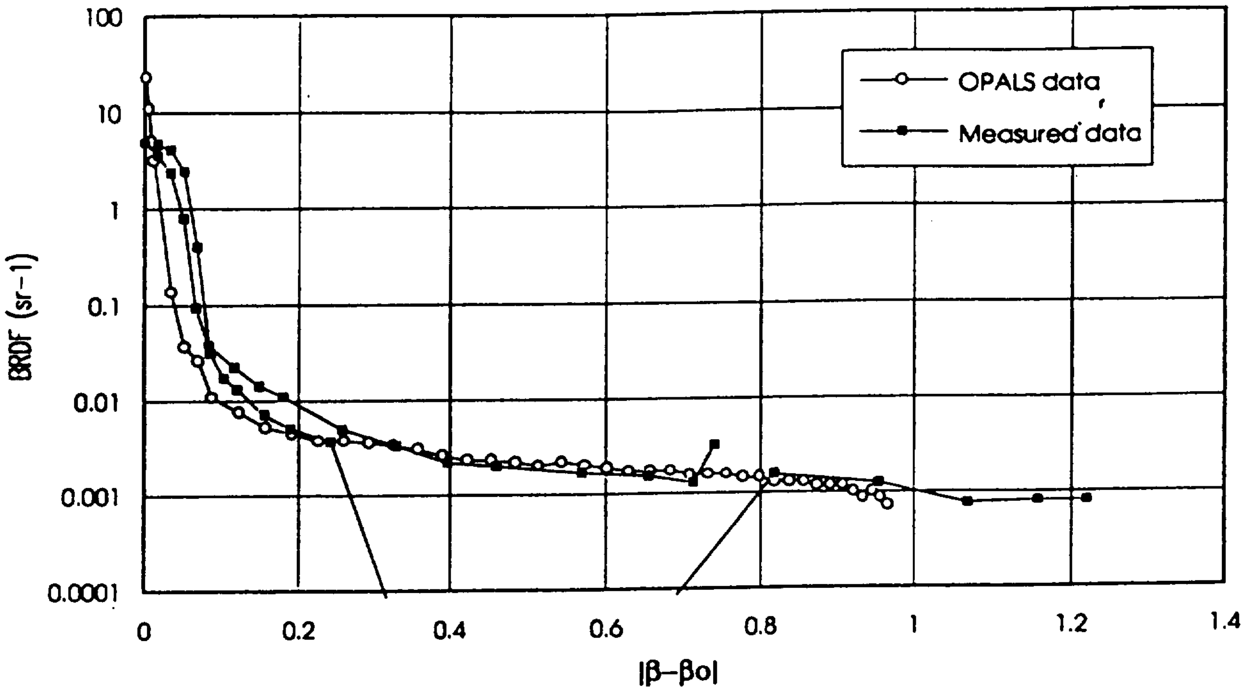

Figure 5 - Measured and theoretical data for 74.0nm and -15 degree angle of incidence. The measured data shows both positive and negative $\beta-\beta_0$.

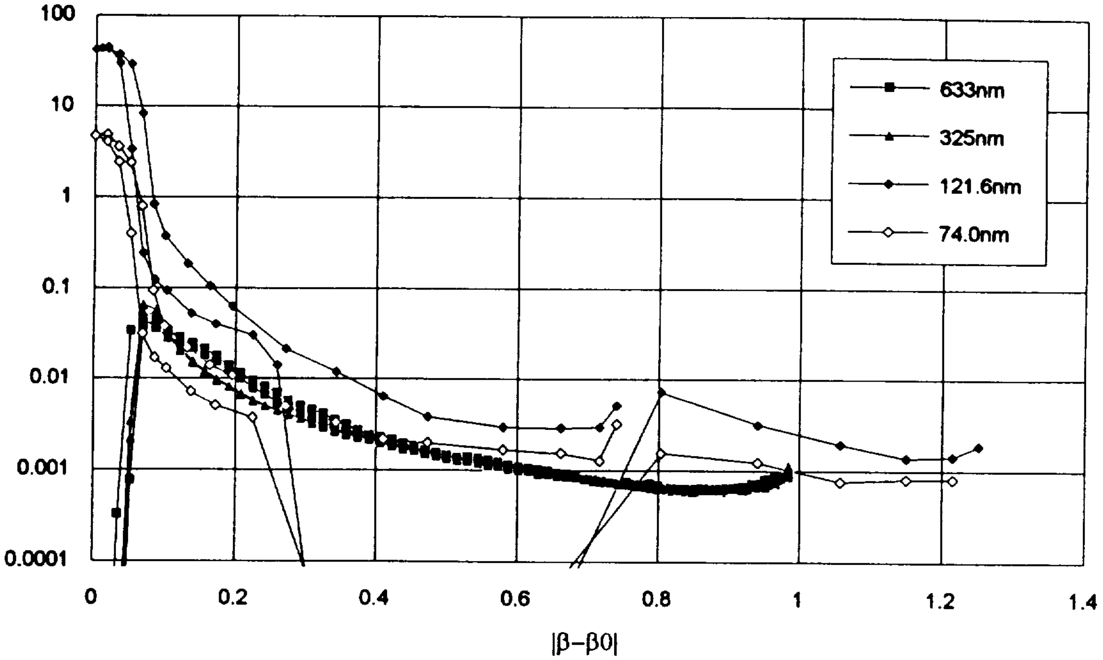

Figure 6 - Measured BRDF data for the same sample at four different wavelengths. Data are shown for positive and negative $\beta - \beta_0$.

Conclusion

In summary, an EUV scatterometer of our own design and construction was used to measure the BRDF of a dust-contaminated mirror at 6328, 3250, 1216, and 740 Å. Comparisons were made with the OPALS modelling software. Agreement with the model was good for the 6328, 3250, and 740 Å measurements, and was fair for the 1216 Å measurements. The 6328, 3250, and 740 Å data suggest that the BRDF may be wavelength-independent, but the 1216 Å measurements do not bear this out. Further investigation is required to determine the wavelength dependence (or lack thereof) of the BRDF.

OPTICAL EFFECTS OF MOLECULAR CONTAMINATION

Molecular contamination can have a devastating effect on the reflectance of UV optics, since most molecular contaminants are very absorptive in the UV. Figure 7, taken from some related work we did, demonstrates this by showing the reflectance loss of the pickoff mirror for the Wide Field Planetary Camera I on the Hubble Space Telescope.

When measuring the reflectance degradation of molecularly-contaminated optics, it is important to distinguish between optics which have been exposed to solar UV and those which have not. While any molecular contaminant on a mirror tends to lower the UV reflectance, experiments and flight data published by several authors[11,12,13,14] have shown that the UV reflectance is especially degraded when the contaminated mirror is exposed to sunlight or other extreme ultraviolet radiation of sufficient intensity. The effect is seen regardless of whether the sunlight is incident on the mirror during the contamination process or whether it illuminates the mirror after contamination. Furthermore, the contaminant becomes "fixed" to the surface; i.e. its vapor pressure decreases to the point that it is no longer possible to remove the contaminant by vacuum bakeout.

This "fixing" of molecular contaminants (especially hydrocarbons) to a surface by UV radiation is believed to be a photopolymerization process; that is, the UV radiation breaks bonds in the hydrocarbon chain and stimulates intermolecular crosslinking. Once the molecules are crosslinked, the energy needed to remove the molecules from the surface becomes prohibitively high.

We have measured the effect of both polymerized and unpolymerized molecular contamination on FUV reflectance. Our samples serving as substrates for contamination were mirrors containing an aluminum + magnesium flouride coating. The mirror samples were contaminated in a controlled fashion using the Contamination Irradiation Facility in the Optics Branch.

Figure 7. UV Reflectance at Normal Incidence

Flight and Spare Pickoff Mirrors

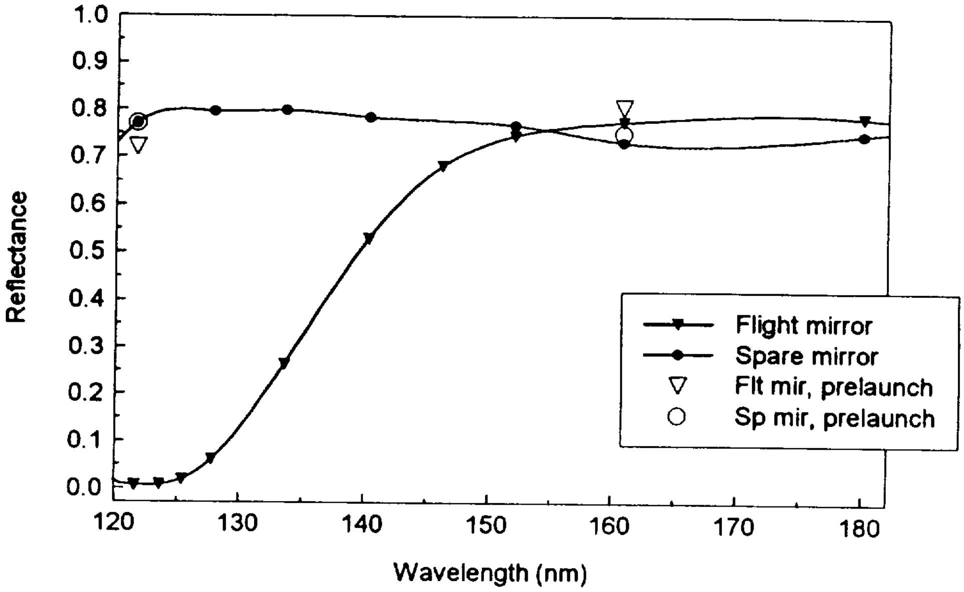

Contamination Irradation Facility

The Contamination Irradiation Facility (CIRF) is designed to perform in-situ measurements of the specular reflectance of contaminated optical surfaces at far-ultraviolet wavelengths (1200-2000 Å). The CIRF is a cryopumped ultra-high vacuum chamber equipped with a McPherson 0.3 meter scanning monochromator for measuring the in-situ specular reflectance of contaminated mirrors. Figure 8 provides a detailed schematic diagram of the CIRF.

The next few paragraphs describe the components of the CIRF and the test procedure for measuring the contaminated samples. Before a sample is mounted in the CIRF, the absolute reflectance of the sample is measured in a Minuteman 302VM monochromator. The absolute reflectance of a reference mirror in the CIRF optical train is also measured. The sample is then mounted in the CIRF on a Huntington Labs 3-axis precision sample manipulator. As shown in Figure 5, the 3-axis precision sample manipulator is needed to rotate the sample 90 degrees after contamination for in-situ reflectance measurements. Once the sample and control mirror are mounted, the chamber is sealed and evacuated down to pressures on the 10^{-7} to 10^{-8} Torr scale. These low pressures are needed to maintain a high level of cleanliness free from contamination and to simulate a spacecraft environment. The pressure level and constituent gases in the chamber are monitored with an ion gauge and a residual gas analyzer (RGA), respectively.

Before contaminating the sample, its specular reflectance is measured in-situ at the same wavelengths mentioned above. These reflectance measurements are performed by a 0.3 m scanning monochromator that is attached, via a MgF_2 window, to the CIRF chamber. The MgF_2 window permits the transmission of ultraviolet radiation above 1150 Å. A Platinum-Neon hollow cathode lamp is used a the source for the reflectance measurements due to its rich spectrum in the 1150-3100 Å region, and a photomultiplier tube with a bialkali photocathode is used as the detector. Before entering the CIRF chamber, the UV light from the Pt-Ne lamp is monitored with a chopper and Cs-Te photomultiplier tube to record any variations in the lamp output. Both the monochromator and optical train assembly are maintained at a pressure of $\sim 10^{-3}$ Torr.

After the uncontaminated in-situ reflectance measurements are completed, the sample is contaminated in a controlled fashion using an effusion cell. As the contaminant is evaporated onto the mirror sample, the deposition rate is monitored in real-time by a quartz crystal thin film deposition monitor. The temperature of the deposition monitor is controlled at approximately 20°C. After a prescribed layer of contaminant has accumulated, the reflectance of the sample is again measured in-situ. The sample is then exposed to intense UV radiation from a Deuterium lamp in order to induce photopolymerization of the contaminant. A Nitric-Oxide ionization chamber detector is used to monitor the deuterium lamp output in terms of equivalent solar hours. Once the sample is sufficiently irradiated and the contaminant is photopolymerized, another in-situ specular reflectance measurement of the contaminated sample is made. Finally, the reference and sample mirrors are removed from the chamber and transferred to the

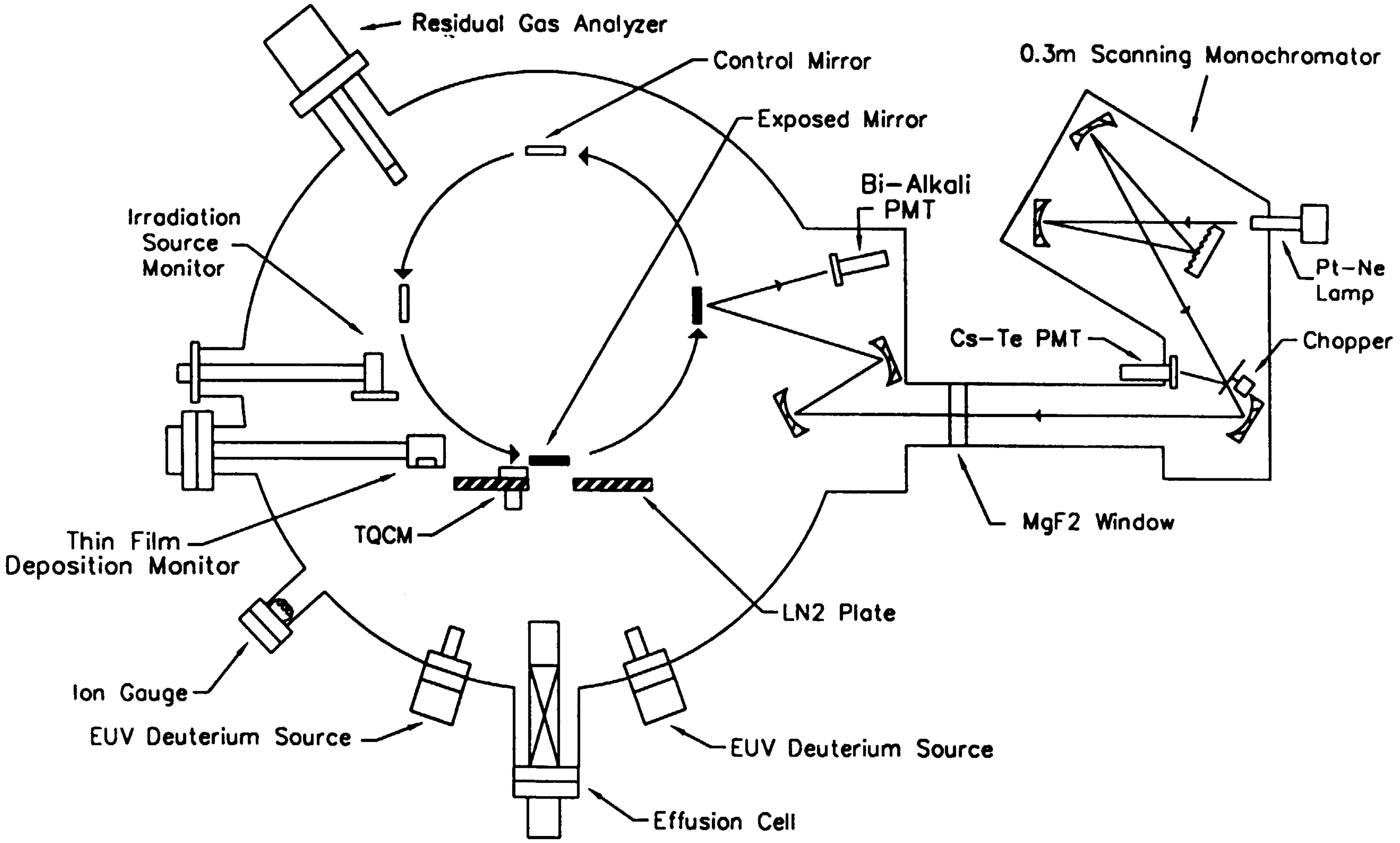

Figure 8 – Schematic Diagram of Contamination Irradiation Facility.

Minuteman 302VM monochromator to measure their absolute reflectance after contamination.

Results

As mentioned above, the samples used for this research were aluminum + magnesium fluoride (Al+MgF_2) mirrors. Al+MgF_2 was chosen because it is the most commonly used coating in the far ultraviolet spectral region down to 1150 Å because of its high reflectivity. The thickness of MgF_2 is carefully selected to eliminate oxidation of the aluminum film while maintaining its high FUV reflectance. Recent applications of this coating include mirrors on Corrective Optics Space Telescope Axial Replacement (COSTAR) and Space Telescope Imaging Spectrograph (STIS). For a coating optimized for 1216 Å the physical thickness of the MgF_2 is 250 Å, which corresponds to an optical halfwave thickness at 1216 Å and an optical quarterwave thickness at 1824 Å.

The contaminant selected for the first test was Hysol epoxy EA9394, an epoxy used for mounting optical mirrors. The effusion cell containining the epoxy was heated to a temperature of 250°C. This high temperature was chosen because the epoxy proved to be so low outgassing that it was not possible to deposit a contaminant at lower temperatures. After several hours the deposition monitor indicated a deposit thickness of 20 Å. An in-situ reflectance measurement of the contaminated mirror was performed at 1216, 1608, and 2000 Å. No change was detected in the reflectance of the contaminated mirror at these wavelengths compared to its uncontaminated values. The sample was then exposed to radiation from one deuterium lamp for a period of 3.5 hrs, to photopolymerize the contaminant. (One deuterium lamp had an intensity at 1216Å of approximately 3 suns.) The reflectance was then remeasured in-situ.

The results of these in-situ reflectance measurements are shown in Figure 9. The top curve is the reflectance before contamination, and the bottom curve is the reflectance after contamination and irradiation. The data indicate a reflectance loss of 0.03 at 1216Å, gradually increasing to a loss of 0.13 at 2000 Å. A larger difference is observed at the longer wavelengths because this region encompasses an effective quarterwave in the MgF_2 coating. Earlier studies[12] have shown that when the MgF_2 layer is an effective quarterwave thick the intrinsic absorption of the surface contaminant is more strongly coupled in the reflected wave than when the MgF_2 layer is an optical halfwave thick. This results in a larger decrease in reflectance in the spectral region where the MgF_2 layer is an effective quarterwave thick.

Before we could take in-situ data using other contaminants, we had an unfortunate accident with the CIRF that destroyed our in-situ measurement capability. Efforts to correct the problem have been underway for almost a year, but so far we have not been able to restore the capability to the point of making publication-quality measurements. Therefore the rest of the data presented herein are reflectance measurements taken just

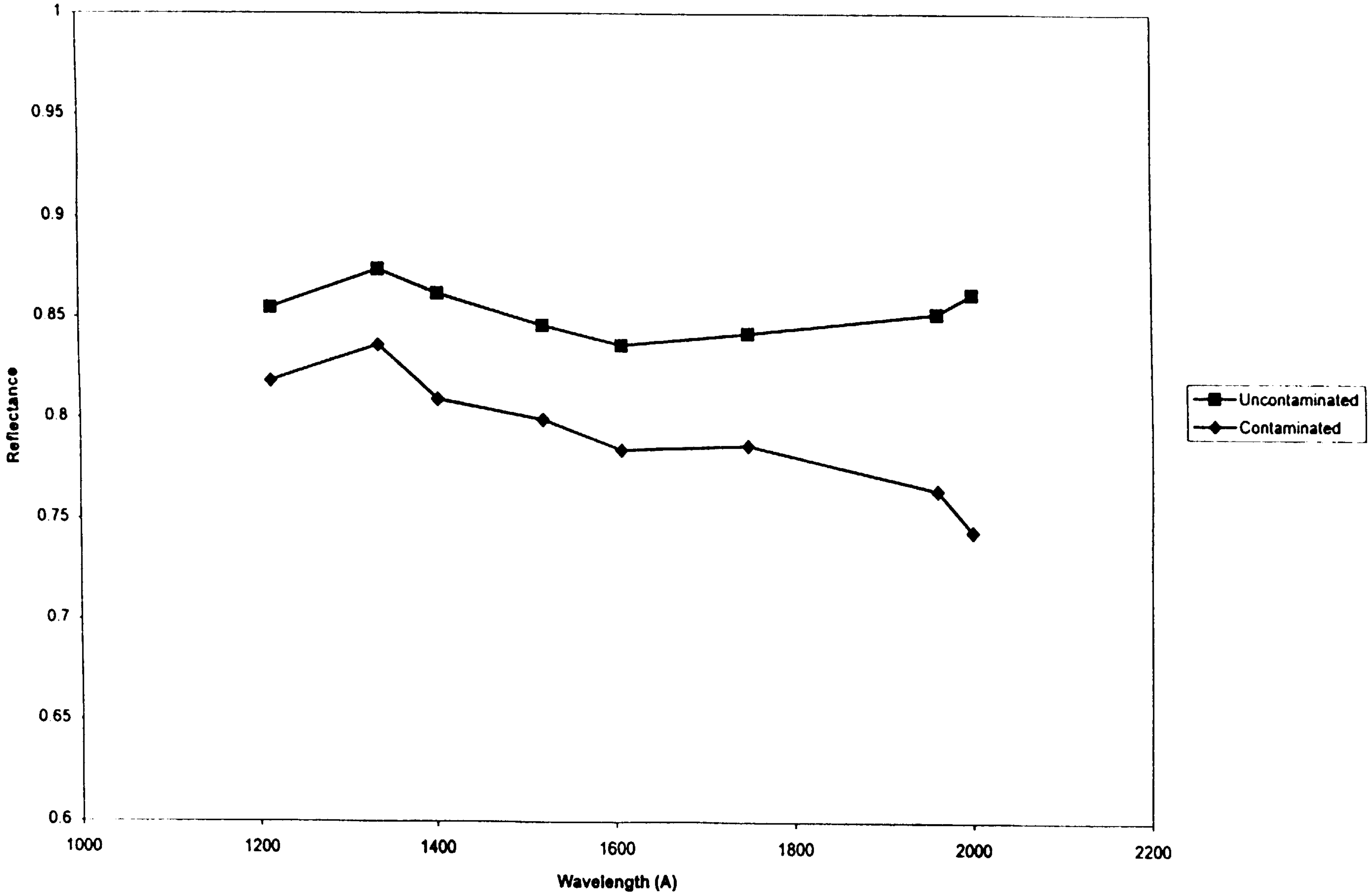

Figure 9 – In-situ reflectance measurements of an Al + MgF_2 mirror before contamination and after contamination + irradiation. Measurements were also made after contamination but before irradiation, and no change in reflectance was seen compared to the uncontaminated state.

before the sample was installed in the chamber and just after the sample was removed from the chamber (after both contamination and irradiation had been performed.)

The following measurements were done in two groups. In the first group, the contamination source was raised to a high temperature (~ 100°C) to drive off as much contamination as possible, the irradiation was for a short time (3.5 hr) using two deuterium lamps, and the irradiation occurred after the contaminant was deposited. In the second group, the contamination source was raised to lower temperatures (40-50°C) to more realistically simulate spacecraft conditions, and the irradiation was for a longer time (~ 20 hr) using two deuterium lamps. Also, because we were having problems getting contamination to deposit on the room-temperature samples, the irradiation was performed simultaneously with the contamination deposition in order to encourage any molecules that struck the sample to stick to it permanently. It didn't seem to make much difference; the amount of deposition achieved in the two groups was about the same.

Before any reflectance drop due to contamination can be interpreted, it is important to establish the "background" reflectance drop seen when no contamination is introduced but irradiation is performed. Ideally this background should be zero, but there is always a small amount of condensible material present in the chamber, either free floating in space or on the chamber walls. Wiping down the chamber walls, baking out the chamber, and pumping to the lowest pressure attainable all help to reduce the amount of such material, but it could not be eliminated entirely. When the sample is irradiated, any condensible molecules which impinge on the sample stick there permanently. The longer the irradiation time, the more molecules accumulate and the bigger the "background" reflectance drop is. This effect is shown in Figure 10 and Figure 11. In Figure 10, the empty effusion cell was heated to 102°C, in case the effusion cell itself could be a source of contamination. Simultaneously the sample was irradiated for 3.5 hr. Very little effect was seen except at the longer wavelengths, where a drop of ~ 0.06 was apparent. In Figure 11, the empty effusion cell was not heated, and the sample was irradiated for 20 hr. A larger effect was seen, attaining a maximum drop of ~ 0.10 at 2000Å. This larger effect suggests that it doesn't make any difference whether the effusion cell is heated; what counts is the irradiation time. This makes sense, since the longer the sample is irradiated, the more opportunity molecules have to impinge on the sample and stick there. The fact that the effect in both cases is stronger at the longer wavelengths is due to the quarter-wave interference effect mentioned above.

The first contaminant used was Epon 815C/ Versamid 140 epoxy, as shown in Figure 12. It was heated to 103°C, and resulted in a contamination layer thickness of 19Å. This deposited contaminant was then irradiated for 3.5 hr. Except for a slight drop at 1216Å, which was within the experimental error, this contamination layer had no effect on the reflectance beyond the background.

Figure 13 shows the results of the next contamination run using Braycote 601 grease. Despite heating it to 105°C, only 5Å of contaminant was able to be deposited on the room-temperature sample. The sample was then irradiated for 3.5 hr. Again there is a

Figure 10

Reflectance change of Al + MgF2 mirror

No contaminant introduced

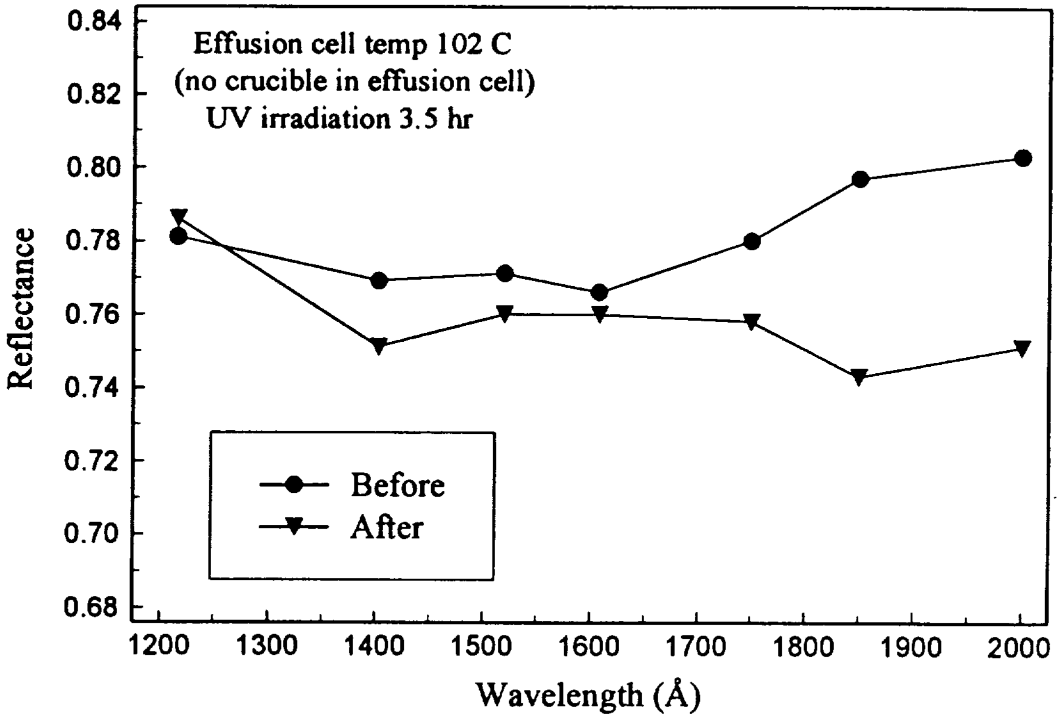

Figure 11

Reflectance change of Al + MgF2 mirror

No contaminant introduced

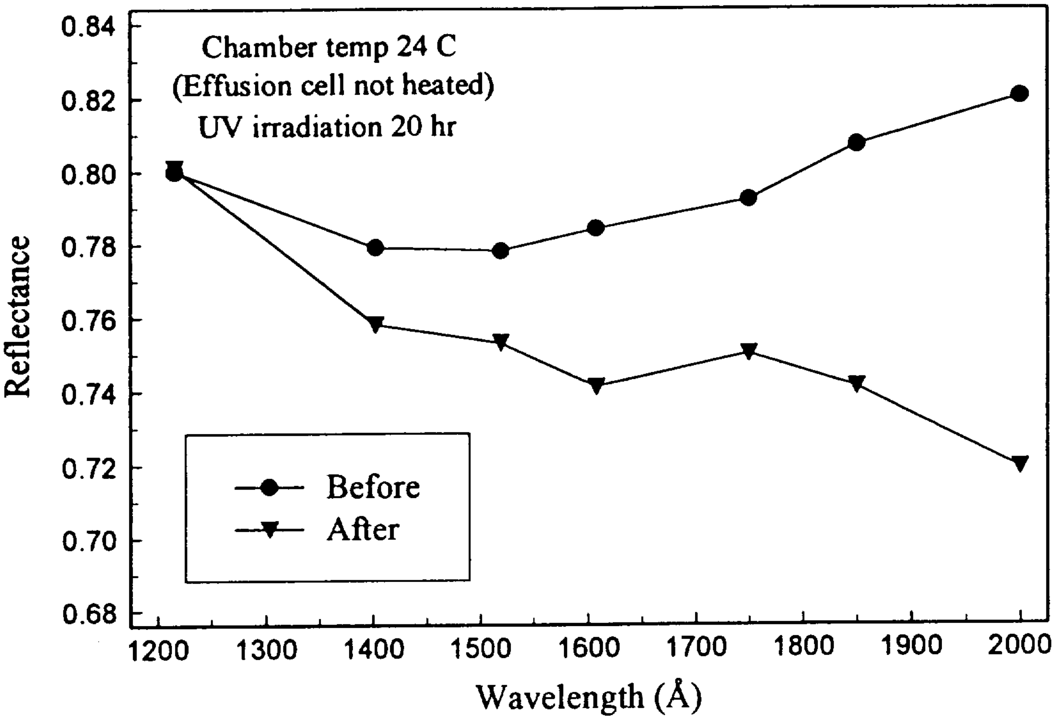

Figure 12

Reflectance change of Al + MgF2 mirror

Contaminant: Epon 815C/Versamid 140

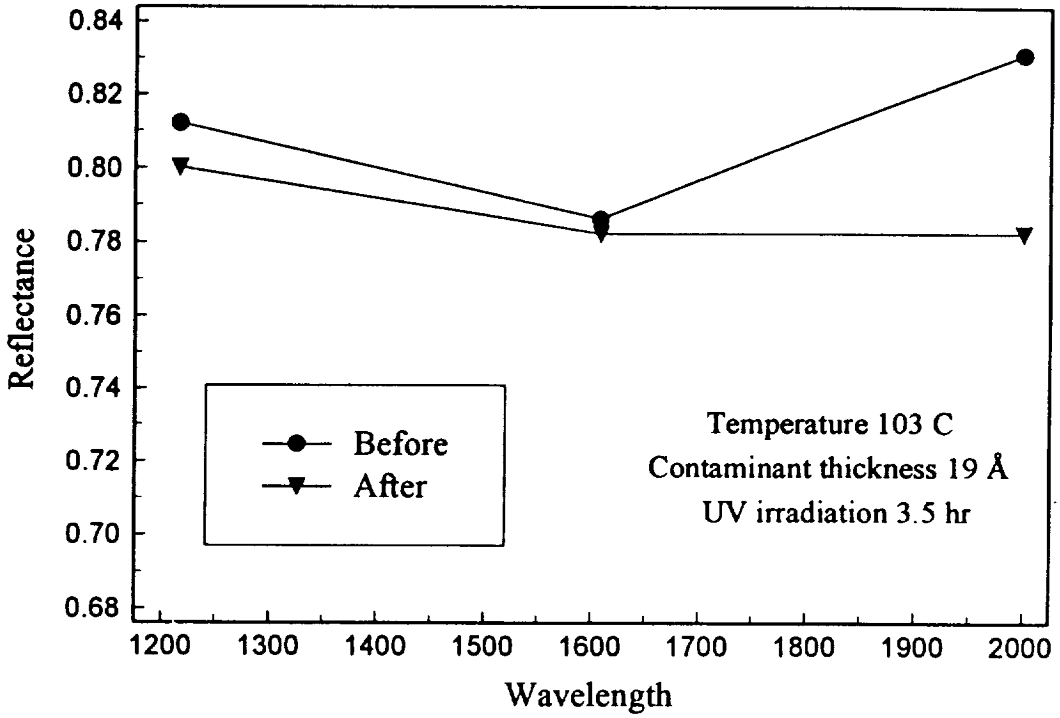

Figure 13

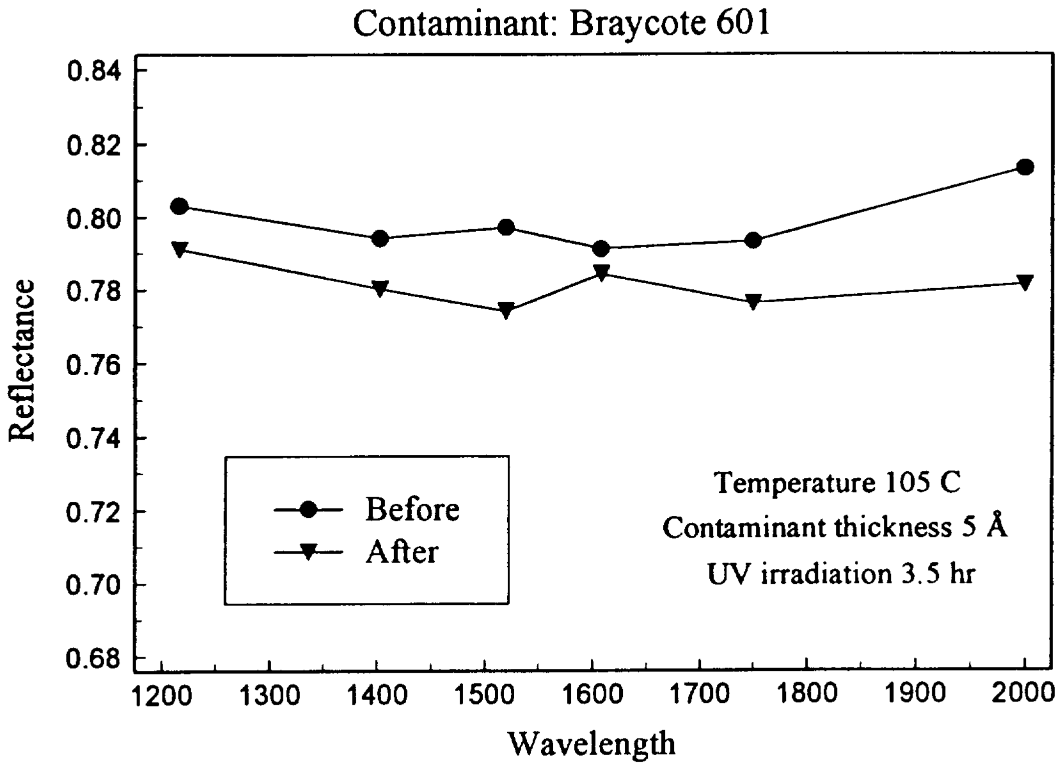
Reflectance change of Al + MgF2 mirror
Contaminant: Braycote 601
Reflectance
0.84
0.82
0.80
0.78
0.76
0.74
0.72
0.70
0.68
1200
1300
1400
1500
1600
1700
1800
1900
2000
Wavelength
● Before
▼ After
Temperature 105 C
Contaminant thickness 5 Å
UV irradiation 3.5 hr

slight effect, within the experimental error, at 1216Å. The only significant reflectance loss occurs at 1520Å. Everywhere else, the reflectance change is within the background. It turns out that all the contaminated samples for which the 1520Å line was measured show a small reflectance drop there. This is interesting, but as the effect is so small (in the noise in some cases), it is difficult to conclude anything from it.

It was noted with the Hysol measurements above that no change in reflectance was seen after the contaminant was deposited on the sample, but before irradiation. It would appear that the same is true for the Epon/Versamid and Braycote runs; even after 3.5 hours of irradiation very little change is seen.

Figure 14 shows the results of the first contamination run with longer irradiation times, using Rheolube 2000 oil with lead napthanate additive. It was heated to 42°C and held there for 20.5 hr while simultaneously being irradiated. A contaminant thickness of 10Å was deposited. Even when compared to the relatively large background, a significant drop in reflectance was seen at almost all wavelengths, most notably 1216, 1520, and 1850Å. The drop at 1850Å is due to the quarter-wave interference effect. The drop at 1216Å is not an interference effect, but rather indicates a contaminant with a fairly strong absorptive index.

The next run, illustrated in Figure 15, involved Pennzane X-2000 oil. It was heated to 52°C, and simultaneously irradiated for 22.5 hr. A contaminant thickness of 20Å was obtained. The only significant reflectance loss compared to the background is at 1216Å. This contaminant therefore also shows a strong absorptive index, though not as strong as the Rheolube, since the Rheolube run showed about the same size drop at 1216Å when there was only half as much contamination present as in the Pennzane run.

The final contamination run, shown in Figure 16, used Krytox 240 AC grease. After being held at 48°C while irradiated for 23.5 hr, a contaminant thickness of 20Å was deposited. A slight reflectance drop at 1216Å is seen, but it is within the experimental error. Significant losses are seen at 1520, 1750, and 1850Å. This contaminant evidently is not as absorptive as the previous two, but does have a refractive index different enough from the sample to cause the quarter-wave interference effect.

Conclusion

In summary, we have measured the contamination-induced reflectance loss of aluminum + magnesium fluoride sample mirrors at wavelengths from 1216 to 2000Å. The contamination layer thicknesses ranged from 5Å to 20Å. In the one case where we could measure the reflectance after contamination but before irradiation, no change in reflectance due to the contaminant alone was detected. After that sample was irradiated for 3.5 hours, a reflectance drop was seen across the board, with the maximum drop of

Figure 14

Reflectance change of Al + MgF2 mirror

Contaminant: Rheolube 2000

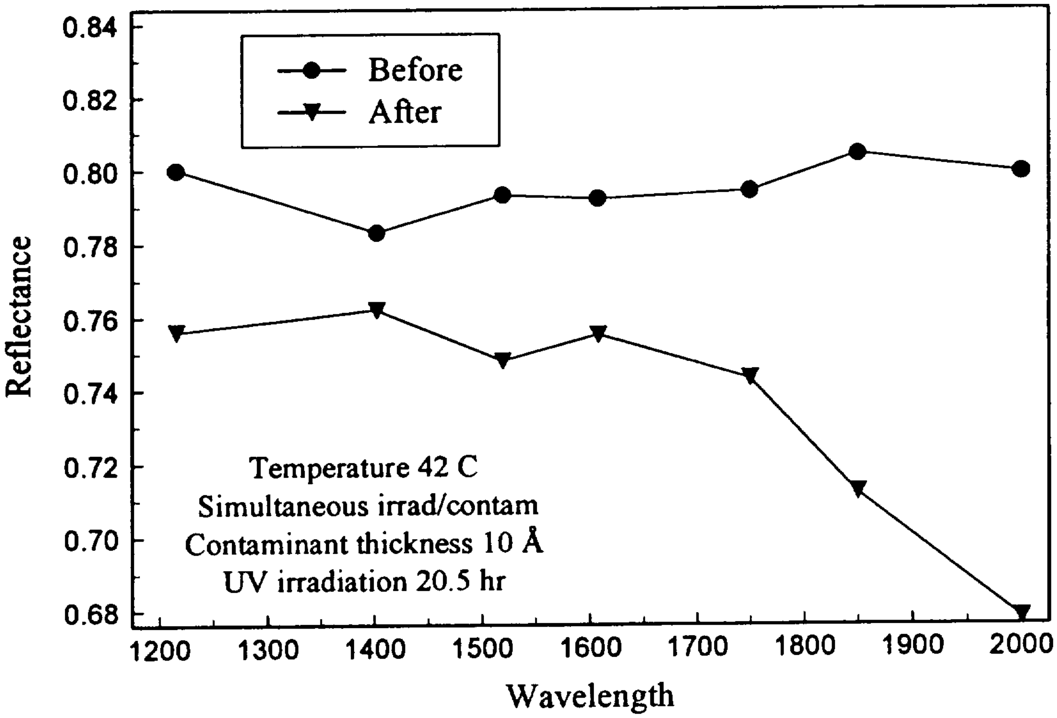

Figure 15

Reflectance change of Al + MgF2 mirror

Contaminant: Pennzane X-2000

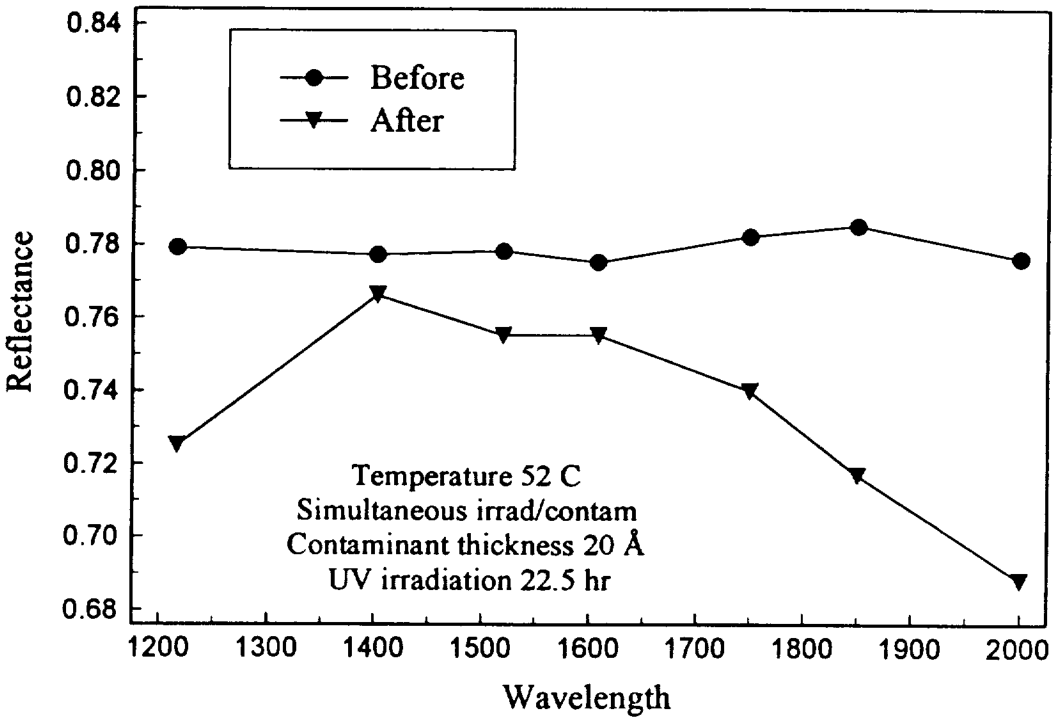

Figure 16

Reflectance change of Al + MgF2 mirror
Contaminant: Krytox 240 AC

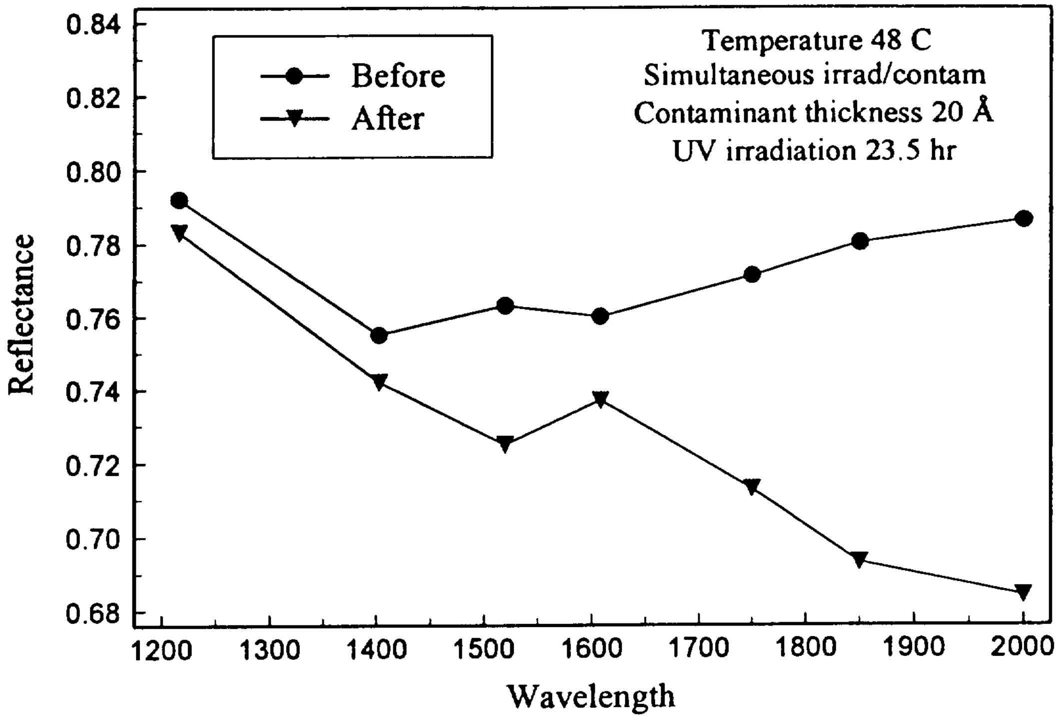

0.13 ocurring at 2000Å. That the maximum loss should happen at longer wavelengths makes sense due to a quarter-wave interference effect.

Of the three samples that were irradiated for 3.5 hours, only the one contaminated with Hysol EA9394 epoxy outgassing products showed a reflectance loss larger than the "background" loss seen when a sample is irradiated for 3.5 hours in the absence of an introduced contaminant.

Of the three samples that were irradiated for approximately 20 hours, the one contaminated using Rheolube 2000 oil showed the largest effect compared to the background. This was true despite the fact that only 10Å of this contaminant was deposited, while the other two samples each accumulated 20Å of contamination. The Rheolube outgassing products proved to have a high absorptive index at 1216Å, as well as causing the quarter-wave interference effect at longer wavelengths. The sample contaminated using Pennzane X-2000 oil showed a sizeable drop at 1216Å, indicating a fairly high absorptive index at that wavelength, but did not significantly affect the reflectance at other wavelengths. The sample contaminated using Krytox 240 AC grease did not have the high absorption at 1216Å, but did have a refractive index different enough from the substrate to cause the quarter-wave interference effect at longer wavelengths.

Although the samples which were irradiated for 3.5 hours were contaminated by heating the contamination source to high temperatures (where one would expect more condensible outgassing products to be driven off), the effect on reflectance was small. The samples that were irradiated for ~20 hours, on the other hand, showed a larger effect even though they were contaminated by heating the contamination source to lower temperatures. Thus the temperature of the outgassing did not seem to matter much. The amount of irradiation was the determining factor in changing the FUV reflectance.

References

1. "Scatter from particulate-contaminated mirrors. Parts 1 - 4", P.R. Spyak and W.W. Wolfe, Optical Engineering 31, 1746. (1992)

2. "Role of scattering distribution functions in spacecraft contamination control practices", P.A. Carosso and N.J.P. Carosso, Applied Optics 25, 1230. (1986)

3. "Low scatter mirror degradation by particle contamination", R.P. Young, Optical Engineering 15, 516. (1976)

4. "PEARLSS, A Model for Contamination Effects: Description and Results", L.A. Whitlock and J.L. Jackson, SPIE 1753, Stray Radiation in Optical Systems II, 136. (1992)

5. "Extreme ultraviolet scatterometer: design and capability", M.P. Newell and R.A.M. Keski-Kuha, Applied Optics 36, 2897. (1997)

6. "On the cause of errors in reflectance vs. angle of incidence measurements and the design of reflectometers to eliminate the errors", W.R. Hunter, Applied Optics 6, 2140. (1967)

7. "Simulation of effects of particulates in the near field-of-view on spaceborne sensor performance", L.A. Whitlock and J.L. Jackson, Surveillance Technologies II, SPIE vol. 1693. (1992)

8. "Extreme ultraviolet scatter from particulate contaminated mirrors, M.P. Newell, L.A. Whitlock, R.A.M. Keski-Kuha, and J.L. Jackson, in *Optical Scattering in the Optics, Semiconductor, and Computer Disk Industries*, J.C. Stover, ed., Proc. SPIE 2541, 174-185. (1995)

9. "Bidirectional reflectance distribution function of diffuse extreme ultraviolet scatterers and extreme ultraviolet baffle materials", M.P. Newell and R.A.M. Keski-Kuha, Applied Optics 36. (1997)

10. "Optical Scattering: Measurement and Analysis, p. 116, McGraw-Hill. (1990)

11. "Laboratory Experiments to Study Surface Contamination and Degradation of Optical Coating and Materials in Simulated Space Environments", G. Hass and W.R. Hunter, Applied Optics 9, 2101. (1970)

12. "Auger spectroscopic examination of MgF_2-coated Al mirrors before and after UV irradiation", J.B. Heaney, H. Herzig, and J.F. Osantowski, Applied Optics 16, 1886. (1977)

13. "Photo-Enhanced Spacecraft Contamination Deposition", D.F. Hall, T.B. Stewart, and R.R. Hayes, AIAA 85-0953. (1985)

14. "Photochemical Spacecraft Self-Contamination: Laboratory Results and Systems Impacts", T.B. Stewart et al., AIAA 88-2728. (1988)

REPORT DOCUMENTATION PAGE

Form Approved
OMB No. 0704-0188

1. AGENCY USE ONLY *(Leave Blank)*	**2. REPORT DATE** June 1999	**3. REPORT TYPE AND DATES COVERED** Technical Publication

4. TITLE AND SUBTITLE
Contamination Effects on EUV Optics

5. FUNDING NUMBERS

6. AUTHORS
J. Tveekrem

7. PERFORMING ORGANIZATION NAMES(S) AND ADDRESS(ES)

NASA Goddard Space Flight Center
Greenbelt, MD 20771

8. PERFORMING ORGANIZATION REPORT NUMBER
M–926

9. SPONSORING/MONITORING AGENCY NAME(S) AND ADDRESS(ES)

NASA's Space Environments and Effects (SEE) Program
George C. Marshall Space Flight Center
Marshall Space Flight Center, Alabama 35812

10. SPONSORING/MONITORING AGENCY REPORT NUMBER
NASA/TP—1999–209264

11. SUPPLEMENTARY NOTES
The SEE Program had a task agreement with GSFC as part of the 1994 NRA. As a result of the task agreement, the deliverable to the SEE Program was a final report. All funded tasks are distributed by the SEE Program.
Technical monitor: Mr. Phil Chen, NASA/GSFC/Code 724.4, (301) 286–8651

12a. DISTRIBUTION/AVAILABILITY STATEMENT

Unclassified/Unlimited
Subject Category 29
Standard Distribution

12b. DISTRIBUTION CODE

13. ABSTRACT *(Maximum 200 words)*

During ground-based assembly and upon exposure to the space environment, optical surfaces accumulate both particles and molecular condensibles, inevitably resulting in degradation of optical instrument performance.

Currently, this performance degradation (and the resulting end-of-life instrument performance) cannot be predicted with sufficient accuracy using existing software tools. Optical design codes exist to calculate instrument performance, but these codes generally assume uncontaminated optical surfaces. Contamination models exist which predict approximate end-of-life contamination levels, but the optical effects of these contamination levels can not be quantified without detailed information about the optical constants and scattering properties of the contaminant. The problem is particularly pronounced in the extreme ultraviolet (EUV, 300–1,200 Å) and far (FUV, 1,200–2,000 Å) regimes due to a lack of data and a lack of knowledge of the detailed physical and chemical processes involved. Yet it is in precisely these wavelength regimes that accurate predictions are most important, because EUV/FUV instruments are extremely sensitive to contamination.

14. SUBJECT TERMS
contamination on optics, EUV effects on optics, contamination, optics

15. NUMBER OF PAGES
34

16. PRICE CODE
A03

17. SECURITY CLASSIFICATION OF REPORT Unclassified	**18. SECURITY CLASSIFICATION OF THIS PAGE** Unclassified	**19. SECURITY CLASSIFICATION OF ABSTRACT** Unclassified	**20. LIMITATION OF ABSTRACT** Unlimited

NSN 7540-01-280-5500

Standard Form 298 (Rev. 2-89)
Prescribed by ANSI Std. 239-18
298-102